

# SCIENTIFIC REPORTS



OPEN

## Morphology of Immunomodulation in Breast Cancer Tumor Draining Lymph Nodes Depends on Stage and Intrinsic Subtype

Maximilian Seidl<sup>1,2,3,13</sup>, Moritz Bader<sup>1,4</sup>, Astrid Vaihinger<sup>1,13</sup>, Ulrich F. Wellner<sup>5</sup>, Romyana Todorova<sup>1,13</sup>, Bettina Herde<sup>1,13</sup>, Klaudia Schrenk<sup>1,2,13</sup>, Jochen Maurer<sup>6</sup>, Oliver Schilling<sup>7,8,9</sup>, Thalia Erbes<sup>12,13</sup>, Paul Fisch<sup>1,13</sup>, Jens Pfeiffer<sup>10,13</sup>, Linda Hoffmann<sup>14</sup>, Kai Franke<sup>11</sup>, Martin Werner<sup>1,3,7,13</sup> & Peter Bronsert<sup>1,3,7,13</sup>

Cancer research of immune-modulating mechanisms mainly addresses the role of tumor-infiltrating immune cells. Mechanisms modulating the adaptive immune system at the primary activation site – the draining lymph node (LN) – are less investigated. Here we present tumor-caused histomorphological changes in tumor draining LNs of breast cancer patients, dependent on the localization (sentinel LN vs. non-sentinel LN), the tumor size, the intrinsic subtype and nodal metastatic status. The quantitative morphological study was conducted in breast cancer patients with at least one sentinel LN and no neoadjuvant therapy. All LNs were annotated considering to their topographical location, stained for IgD/H&E, digitized and quantitatively analyzed. In 206 patients, 394 sentinels and 940 non-sentinel LNs were categorized, comprising 40758 follicles and 7074 germinal centers. Subtype specific immunomorphological patterns were detectable: Follicular density was higher in LNs of Her2 enriched hormone receptor positive and triple-negative breast cancers whereas hormone receptor positive breast cancers showed more macrophage infiltrations in the LN cortex. Follicles are rounder in metastatic LNs and non-sentinel LNs. The identified immunomorphological changes reflect different underlying immunomodulations taking place in the tumor-draining LNs and should therefore be considered as possible prognostic and predictive markers for LN metastasis and therapy associated immunomodulation.

LN metastasis is crucial in tumor evolution and associated with an adverse outcome in most solid tumors. LNs are organized compartments (marginal sinus, follicle, germinal center, mantle zone) of lymphoid tissue that is passed through by lymph and blood vessels. The LN compartments can concentrate antigens, help to produce corresponding antibodies, and recruit immune cells<sup>1,2</sup>. Depending on the type and amount of the stimulus these compartments can expand or diminish<sup>3–6</sup>. In cancer, tumor draining lymph vessels and endothelial venules

<sup>1</sup>Institute for Surgical Pathology, Medical Center – University of Freiburg, Freiburg, Germany. <sup>2</sup>Center for Chronic Immunodeficiency, Medical Center – University of Freiburg, Freiburg, Germany. <sup>3</sup>Comprehensive Cancer Center Freiburg, Medical Center – University of Freiburg, Freiburg, Germany. <sup>4</sup>Division of Cranio-maxillo-facial Surgery, Department of Reconstructive Surgery, University of Basel, Basel, Switzerland. <sup>5</sup>Clinic for Surgery, University Clinic Schleswig-Holstein Campus Lübeck, Lübeck, Germany. <sup>6</sup>Department of Gynecology, RWTH Aachen University Hospital, Aachen, Germany. <sup>7</sup>German Cancer Consortium (DKTK) and Cancer Research Center (DKFZ), Heidelberg, Germany. <sup>8</sup>Institute for Molecular Medicine and Cell Research, University of Freiburg, Freiburg, Germany. <sup>9</sup>BIOS Centre for Biological Signaling Studies, University of Freiburg, Freiburg, Germany. <sup>10</sup>Department of Oto-Rhino-Laryngology, Medical Center – University of Freiburg, Freiburg, Germany. <sup>11</sup>Department of Trauma, Hand and Reconstructive Surgery Giessen, University Hospital Giessen-Marburg, Giessen, Germany. <sup>12</sup>Department of Obstetrics and Gynecology, Medical Center – University of Freiburg, Freiburg, Germany. <sup>13</sup>Faculty of Medicine, University of Freiburg, Freiburg, Germany. <sup>14</sup>Basler Versicherungen, Basel, Switzerland. Moritz Bader and Astrid Vaihinger contributed equally to this work. Correspondence and requests for materials should be addressed to M.S. (email: [maximilian.seidl@uniklinik-freiburg.de](mailto:maximilian.seidl@uniklinik-freiburg.de))

Received: 20 June 2017

Accepted: 14 March 2018

Published online: 28 March 2018

– triggered by the tumor – are forming the pre-metastatic niche in tumor draining LNs<sup>7,8</sup>. Tumor derived soluble factors, debris and cells converge via lymph vessels, into the local draining LNs. These are expected to build the foundation for LN metastasis<sup>9–12</sup> according to the “seed and soil” hypothesis<sup>13,14</sup>.

The current focus of cancer research in immune-modulating mechanisms mainly addresses the role of tumor-infiltrating immune cells as therapeutic targets (such as the PD1/PDL1 axis)<sup>15,16</sup>, representing the effector site of tumor promoting immunity.

The identification of mechanisms modulating the adaptive immune system at the primary activation site – the draining LN – is fairly out of focus. Data for the amount and spatial allocation of immune cells and their descendants in tumor draining LNs reflecting tumorous immunomodulatory transformations are rare and not matched with tumor infiltrating immune cells<sup>17–21</sup>.

The topographic allocation of the lymph drainage (sentinel/adjacent LNs) in breast cancer represents an ideal model to circumstantiate and trace morphological cancer-based immune modulating effects. In addition, the predictive relevant intrinsic subtyping enables insights into the effects of inter-tumoral heterogeneity on LN compartments.

Our project focused on quantitative histomorphological changes in distinct compartments (follicles, germinal centers with their mantle zone, cortical macrophages) of sentinel and non-sentinel regional LNs of breast cancer patients of different intrinsic subtypes.

## Results

All data supporting the below described findings are available from the corresponding author upon reasonable request.

**Descriptive Statistics.** In 206 patients, 394 sentinel, 512 level I and 428 level II and III LNs were categorized for LN circumference (1515.40–170385.30  $\mu\text{m}$ , median 36512.90  $\mu\text{m}$ ) and area (76017.10  $\mu\text{m}^2$ –338119557.90  $\mu\text{m}^2$ , median 35422800.90  $\mu\text{m}^2$ ), follicle circumference (120.40–18511.00  $\mu\text{m}$ , median 844.00  $\mu\text{m}$ ) and area (946.10  $\mu\text{m}^2$ –6372006.90  $\mu\text{m}^2$ , median 44695.05  $\mu\text{m}^2$ ), germinal center circumference (74.20–12241.10  $\mu\text{m}$ , median 554.75  $\mu\text{m}$ ) and area (399.40  $\mu\text{m}^2$ –2677011.90  $\mu\text{m}^2$ , median 20370.70  $\mu\text{m}^2$ ) and –if present – metastases circumference (276.60–566460.00  $\mu\text{m}$ , median 55372.80  $\mu\text{m}$ ) and area (2060.00  $\mu\text{m}^2$ –269337442.60  $\mu\text{m}^2$ , median 21580975.30  $\mu\text{m}^2$ ). Altogether, we measured 40758 follicles and 7074 germinal centers in 1334 LNs. All patients contained follicles, whereas in 20 patients no germinal centers were detectable. Calculations of the following parameters were based on these findings.

**Univariate Analyses Identify Significant Correlations Between Clinicopathological Parameters and LN morphometry.** Histomorphological parameters were correlated with clinicopathological findings. Follicle and germinal center density, non-circular follicles and germinal centers and cortical macrophage infiltration were analyzed for correlations with age, pT category, nodal status, tumor grading, hormone and Her2 receptor status, and intrinsic subtype, respectively; in all LNs independent of the level (details are listed in Table 1). Patients' age showed a (non-significant) tendency toward rounder germinal centers (Fig. 1A, exemplary).

A higher pT-category was accompanied with a significant ( $p < 0.05$ ) higher follicular and germinal center density as well as smaller mantle zones (Fig. 1A,C, exemplary). On the other hand, a lower pT-category attended significantly more non-circular germinal centers (Fig. 1B, exemplary) and larger mantle zones (represented by a lower mantle zone ratio). Statistical trends ( $p > 0.05$  and  $< 0.15$ ) were observed between pT-category and non-circular follicles as well as cortical macrophage infiltrations (Fig. 1D, exemplary).

Considering the nodal status, an advanced pN-category showed a significantly higher follicular and germinal center density. Higher pN-category showed significantly rounder follicles, rounder germinal centers and smaller mantle zones. Tumor grading/differentiation correlated significantly positive with tumor infiltrating lymphocytes (TILs), an elevated follicular and germinal center density and negative with cortical macrophage infiltration. Statistical trends were observed for non-circular follicles.

Hormone receptor expression for estrogen and progesterone correlated significantly positive with cortical macrophage infiltration and negative with TILs, follicular and germinal center density. Additionally, hormone receptor positive cases tend to have larger mantle zones, progesterone receptor expression revealed a positive statistical trend for non-circular follicles. Considering the Her2 status, a positive statistical trend for follicle density was observed.

**Linear Regression Model Analyses Identify Independent Correlations Between Clinicopathologic Parameters and Morphometrical Data.** Univariate significant correlations and trends (Table 1) were included into a linear regression for multivariate analysis (detailed values are enlisted in Table 2). Considering clinicopathologic parameters, linear regression analyses revealed independent correlations between follicle density and the intrinsic subtype, between tumor grading and follicle roundness as well as between follicle and germinal center roundness and mantle zone ratio. Furthermore, independent correlations between follicle density and germinal center density but also between follicle roundness and germinal center roundness were detected.

**Subtype-specific Analyses Reveal Distinctive Immunomorphological Patterns in the LNs.** For subtype-specific analysis, all morphometric data (follicular and germinal center density, non-circular follicles and germinal centers, mantle zone ratio, cortical macrophages and tumor infiltrating lymphocytes) were included and tested for each intrinsic subtype separately. Follicle density correlated significantly positive ( $p < 0.05$ ) with the luminal-Her2 and triple-negative subtype and significantly negative ( $p < 0.05$ ) with the luminal-A and -B subtypes, respectively. Germinal center density correlated positive with the triple-negative and negative with the luminal-A and -B subtypes. Cortical macrophages and luminal-A and -B subtype demonstrated positive correlations, whereas the luminal-Her2, the Her2-enriched and the triple-negative subtypes correlated significantly

		Follicle Density	Germinal Center Density	Non-circular Follicles	Non-circular Germinal Centers	Mantle Zone Ratio	M $\phi$	TILs
Age	min = 29 max = 87 median = 63	p = 0.618 cc = -0.035	p = 0.486 cc = 0.049	p = 0.256 cc = -0.080	p = 0.094 cc = -0.124	p = 0.288 cc = 0.074	p = 0.368 cc = -0.063	p = 0.864 cc = 0.012
pT	T1 (n = 118)	p < 0.001 cc = 0.260	p < 0.001 cc = 0.239	p = 0.061 cc = -0.131	p = 0.033 cc = -0.157	p = 0.001 cc = 0.228	p = 0.111 cc = -0.111	p = 0.070 cc = 0.127
	T2 (n = 74)							
	T3 (n = 6)							
	T4 (n = 8)							
pN	N- (n = 137)	p = 0.01 cc = 0.178	p < 0.001 cc = 0.223	p = 0.006 cc = -0.189	p = 0.03 cc = -0.160	p = 0.001 cc = 0.225	p = 0.330 cc = -0.068	p = 0.124 cc = 0.108
	N+ (n = 69)							
G	G1 (n = 24)	p < 0.001 cc = 0.302	p < 0.001 cc = 0.276	p = 0.062 cc = -0.131	p = 0.884 cc = 0.015	p = 0.027 cc = 0.154	p < 0.001 cc = -0.237	p < 0.001 cc = 0.292
	G2 (n = 113)							
	G3 (n = 69)							
ER	Negative (n = 54)	p < 0.001 cc = -0.287	p < 0.001 cc = -0.283	p = 0.799 cc = -0.018	p = 0.913 cc = 0.008	p = 0.059 cc = -0.132	p < 0.001 cc = 0.423	p < 0.001 cc = -0.304
	Positive (n = 152)							
PR	Negative (n = 65)	p < 0.001 cc = -0.325	p < 0.001 cc = -0.266	p = 0.051 cc = 0.136	p = 0.390 cc = 0.064	p = 0.146 cc = -0.102	p < 0.001 cc = 0.379	p < 0.001 cc = -0.269
	Positive (n = 141)							
Her2	Score 0 (n = 67)	p = 0.133 cc = 0.105	p = 0.909 cc = -0.008	p = 0.805 cc = 0.017	p = 0.676 cc = -0.031	p = 0.699 cc = -0.027	p = 0.929 cc = 0.006	p = 0.959 cc = -0.004
	Score 1 (n = 96)							
	Score 2 (n = 16)							
	Score 3 (n = 27)							
Subtype	luminal-A (n = 69)	p < 0.001 cc = 0.440	p < 0.001 cc = 0.270	p = 0.443 cc = -0.054	p = 0.650 cc = -0.034	p = 0.143 cc = 0.102	p < 0.001 cc = -0.264	p < 0.001 cc = 0.277
	luminal-B (n = 68)							
	luminal-HER (n = 15)							
	HER2-enriched (n = 12)							
	triple-negative (n = 42)							
Follicle Density	n = 206 min = 7.68* max = 480.11* median = 146.96*	cc = 1.000	p < 0.001 cc = 0.394	p = 0.683 cc = 0.029	p = 0.934 cc = 0.006	p = 0.956 cc = -0.004	p = 0.003 cc = -0.208	p = 0.10 cc = 0.115
Germinal Center Density	n = 206 min = 0* max = 112.97* median = 19.23*	p < 0.001 cc = 0.394	cc = 1.000	p = 0.165 cc = -0.097	p = 0.032 cc = 0.158	p < 0.001 cc = 0.811	p = 0.167 cc = -0.097	p = 0.004 cc = 0.199
Non-circular Follicles	n = 206 min = 1.02 max = 2.07 median = 1.20	p = 0.683 cc = 0.029	p = 0.165 cc = -0.097	cc = 1.000	p < 0.001 cc = 0.433	p < 0.001 cc = -0.245	p = 0.329 cc = 0.068	p = 0.947 cc = 0.005
Non-circular Germinal Centers	n = 186 min = 1.01 max = 2.18 median = 1.09	p = 0.934 cc = 0.006	p = 0.032 cc = 0.158	p < 0.001 cc = 0.433	cc = 1.000	p = 0.458 cc = 0.055	p = 0.725 cc = -0.026	p = 0.172 cc = 0.101
Mantle Zone Ratio	n = 206 min = 0 max = 0.27 median = 0.02	p = 0.367 cc = 0.063	p < 0.001 cc = 0.802	p = 0.455 cc = 0.052	p = 0.001 cc = 0.247	cc = 1.000	p = 0.679 cc = -0.029	p = 0.014 cc = 0.171
M $\phi$	n = 206 absent = 168 present = 38	p = 0.003 cc = -0.208	p = 0.167 cc = -0.097	p = 0.329 cc = 0.068	p = 0.725 cc = -0.026	p = 0.766 cc = 0.021	cc = 1.000	p = 0.018 cc = -0.164
TILs	N = 206 Absent = 134 Present = 72	p = 0.10 cc = 0.115	p = 0.004 cc = 0.199	p = 0.947 cc = 0.005	p = 0.172 cc = 0.101	p = 0.014 cc = 0.171	p = 0.018 cc = -0.164	cc = 1.000

**Table 1.** Univariate analyses for all patients. Spearman Rho correlation coefficient (cc) calculation was performed for all items (p value is provided over the cc value). Abbreviations: pT: T-category of the primary tumor; pN: N-category of the primary tumor; G: tumor grading according to Elston and Ellis<sup>66</sup>; ER: estrogen receptor protein positivity as defined by >1% of tumor cell nuclear positivity in immunohistochemical stainings; PR: progesterone receptor protein positivity as defined by >1% of tumor cell nuclear positivity in immunohistochemical stainings; Her2: human epidermal growth factor receptor type 2 positivity according to Wolff *et al.*<sup>68</sup>; follicle density and germinal center density were calculated by number of follicles or germinal centers over lymph node area; calculation of non-circular follicles and germinal centers is described in the methods part; mantle zone ratio was calculated as area ratio of each germinal center over the corresponding follicle; M $\phi$ : cortical macrophage infiltrations as defined in the methods part; TIL: tumor infiltrating lymphocytes as defined in the methods part. Values marked with asterisk are multiplied with 10<sup>-8</sup>.

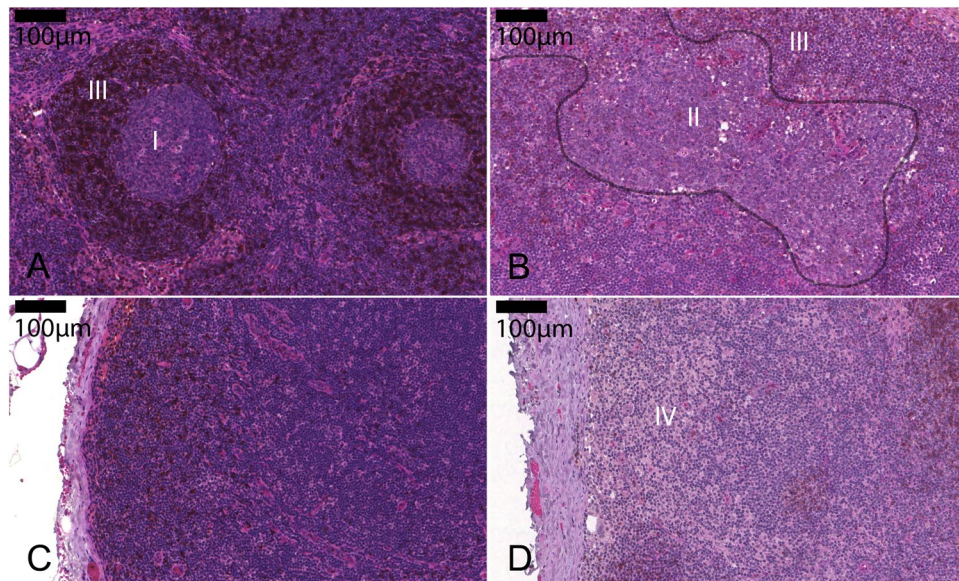


**Figure 1.** Tumor draining lymph nodes display different immunomorphologies. (A) Round germinal center (I) with surrounding IgD+ cells (brown staining) in a well-defined mantle zone (III). (B) Almost “naked” non-circular germinal center (II, highlighted by a grey line) with dim mantle zone (III). (C) Sparsely distributed IgD+ cells (brown staining) in a lymph node with low follicular density. (D) Macrophage infiltration in lymph node cortex (IV). Magnifications as indicated by bar.

	Follicle Density	Germinal Center Density	Non-circular Follicles	Non-circular Germinal Centers	Mantle Zone Ratio	M $\phi$	TILs
Age	n.i.	n.i.	n.i.	n.s.	n.i.	n.i.	n.i.
pT	n.s.	n.s.	n.s.	n.s.	n.s.	n.s.	n.s.
pN	n.s.	n.s.	n.s.	n.s.	n.s.	n.i.	n.s.
G	n.s.	n.s.	<b>p = 0.045</b>	n.i.	n.s.	n.s.	n.s.
ER	n.s.	n.s.	n.i.	n.i.	n.s.	n.s.	n.s.
PR	n.s.	n.s.	n.s.	n.i.	n.s.	n.s.	n.s.
Her2	n.i.	n.i.	n.i.	n.i.	n.i.	n.i.	n.i.
Subtype	<b>p = 0.001</b>	n.s.	n.i.	n.i.	n.s.	n.s.	n.s.
Follicle Density	n.i.	n.s.	n.i.	n.i.	n.i.	n.s.	n.s.
Germinal Center Density	<b>p &lt; 0.001</b>	n.i.	n.i.	n.s.	<b>p &lt; 0.001</b>	n.i.	n.s.
Non-circular Follicles	n.i.	n.i.	n.i.	n.s.	<b>p = 0.005</b>	n.i.	n.i.
Non-circular Germinal Center	n.i.	n.s.	<b>p &lt; 0.001</b>	n.i.	n.i.	n.i.	n.i.
Mantle Zone Ratio	n.i.	n.s.	n.i.	n.s.	n.i.	n.i.	n.s.
M $\phi$	n.s.	n.i.	n.i.	n.i.	n.i.	n.i.	n.i.
TILs	n.s.	n.s.	n.i.	n.i.	n.s.	n.s.	n.i.

**Table 2.** Multivariate linear regression model overall patients with a significant p-value ( $p < 0.05$ ) or statistical trend ( $p > 0.05$  and  $< 0.150$ ) in the univariate analyses using Spearman Rho correlation coefficient (Table 1). Abbreviations: pT: T-category of the primary tumor; pN: N-category of the primary tumor; G: tumor grading according to Elston and Ellis<sup>66</sup>; ER: estrogen receptor protein positivity as defined by  $>1\%$  of tumor cell nuclear positivity in immunohistochemical stainings; PR: progesterone receptor protein positivity as defined by  $>1\%$  of tumor cell nuclear positivity in immunohistochemical stainings; Her2: human epidermal growth factor receptor type 2 positivity according to Wolff *et al.*<sup>68</sup>; follicle density and germinal center density were calculated by number of follicles or germinal centers over lymph node area; calculation of non-circular follicles and germinal centers is described in the methods part; mantle zone ratio was calculated as area ratio of each germinal center over the corresponding follicle; M $\phi$ : cortical macrophage infiltrations as defined in the methods part; TIL: tumor infiltrating lymphocytes as defined in the methods part.

negative with the amount of cortical macrophages. Regarding the effector site, TILs correlated negatively with the luminal-A and -B but positively with the triple-negative subtypes, respectively. Statistical trends were observed between germinal center density and Her2-enriched tumors, follicle roundness and triple-negative subtype and

	Follicle Density	Germinal Center Density	Non-circular Follicles	Non-circular Germinal Centers	Mantle Zone Ratio	M $\phi$	TILs
Luminal-A vs. all other subtypes	p = < 0.001 cc = -0.293	p = 0.001 cc = -0.197	p = 0.252 cc = 0.066	p < 0.436 cc = -0.048	p = 0.106 cc = -0.093	p = 0.003 cc = 0.168	p = 0.043 cc = -0.041
Luminal-B vs. all other subtypes	p = < 0.001 cc = -0.232	p = 0.028 cc = -0.125	p < 0.765 cc = -0.017	p = 0.565 cc = -0.035	p = 0.608 cc = -0.029	p = < 0.001 cc = 0.316	p = 0.022 cc = -0.160
Luminal-Her2 vs. all other subtypes	p = < 0.001 cc = 0.202	p = 0.397 cc = 0.049	p = 0.334 cc = 0.055	p = 0.446 cc = -0.047	p = 0.768 cc = 0.017	p = 0.015 cc = -0.139	p = 0.672 cc = -0.030
Her2-enriched vs. all other subtypes	p = 0.763 cc = 0.017	p = 0.106 cc = 0.093	p = 0.233 cc = -0.068	p = 0.158 cc = -0.087	p = 0.104 cc = 0.093	p = 0.003 cc = -0.168	p = 0.262 cc = 0.078
Triple-negative vs. all other subtypes	p = < 0.001 cc = 0.407	p = < 0.001 cc = 0.253	p = 0.145 cc = -0.084	p = 0.273 cc = 0.067	p = 0.271 cc = 0.063	p = < 0.001 cc = -0.336	p < 0.001 cc = 0.286

**Table 3.** Subtype stratified univariate analyses for all patients. Spearman Rho correlation coefficient (cc) calculation was performed for all items (p value is provided over the cc value). Follicle density and germinal center density were calculated by number of follicles or germinal centers over lymph node area; calculation of non-circular follicles and germinal centers is described in the methods part; mantle zone ratio was calculated as area ratio of each germinal center over the corresponding follicle; M $\phi$ : cortical macrophage infiltrations as defined in the methods part; TIL: tumor infiltrating lymphocytes as defined in the methods part.

mantle zone with luminal-A and Her2-enriched tumors. Further results are presented in Table 3, Fig. 2 (absolute numbers of patients are highlighted in Table 4), and visualized in a heatmap (Fig. 3).

**Follicular Density, Follicular Shape, and Cortical Macrophage Infiltrations Differ Between Draining LN Stations and Intrinsic Subtypes.** For the determination of subtype-specific immunomorphological changes in the position-dependent LN draining stations (sentinel LN vs level I-III) morphological differences in sentinel vs non-sentinel LNs were evaluated over all subtypes and for each subtype separately (Table 5, Fig. 2A–D).

Considering all subtypes, follicle density is lower in sentinel vs non-sentinel LNs (positive correlation with higher LN level, Table 5), whereas non-sentinel LNs displayed rounder follicles and germinal centers (negative correlations for non-circular follicles and germinal centers and higher LN level). Cortical macrophage infiltrations were found to be lower in non-sentinel LNs compared to Sentinel LNs.

Specific analyses for each of the intrinsic subtypes showed luminal-A, -B and triple-negative tumors to have significantly rounder follicles and germinal centers in the non-sentinel LNs (negative correlations between follicle and germinal center un-roundness in sentinel vs level I-III LNs, Table 5). The luminal-B subtype demonstrated more cortical macrophages in sentinel LNs compared to non-sentinel LNs (negative correlation between cortical macrophage infiltration and higher LN level, Table 5). The luminal-Her2 subtype also displayed rounder follicles in non-sentinel LNs and a statistical trend for rounder germinal centers (significant negative correlation with non-circular follicles and higher LN levels and statistical trend for negative correlation between non-circular germinal centers and higher LN levels; Table 5).

Further statistical trends ( $p > 0.05$  and  $< 0.15$ ) were observed between luminal-A subtype and follicle density, luminal-Her2 as well as Her2-enriched subtype and germinal center roundness.

## Discussion

Our data demonstrate the immune-modulating effects in tumor draining LNs. The study comprised 206 breast cancer patients with 1334 defined LN stations manually annotated, measured, and analyzed for the presence of macrophages, follicles, germinal centers and LN metastasis. Data was generated with a very high granularity. It can be traced back down to the single follicle of each LN of each patient, and was matched with the primary tumor as immunological effector site. To our knowledge, such a detailed analysis has not been compiled before.

Immune-modulated histomorphological changes in LNs can be summarized into subtype-independent groups (pT and pN) and subtype-dependent groups (tumor grade, estrogen and progesterone receptor protein expression).

Advanced tumor growth, i.e. the pT category, revealed a significant positive correlation with follicular and germinal center density, germinal center roundness, and smaller mantle zones. Using an example, a high pT stage is accompanied by an elevated follicular and germinal center density with quantitatively more round germinal centers and with smaller mantle zones.

On the other hand, hormone receptors as the aforementioned tumor-intrinsic factors demonstrated a significant negative correlation for follicle and germinal center density. Furthermore, they are affecting the presence of tumor infiltrating lymphocytes within the tumor and the cortical macrophages within the LNs: A decrease of the estrogen receptor expression was accompanied with a higher number of tumor infiltrating lymphocytes within the tumor and with a higher follicle and germinal center density. A decrease of the estrogen receptor protein was also accompanied by a lower number of cortical macrophages within the draining LN. Notably, all observed changes were not affected by patients' age.

There are published findings of increased and decreased dendritic cell infiltrations in tumor draining LNs: Laguens *et al.* indicated that the LNs which are draining solid tumors present decreased dendritic cells compared with controls. Their observations are based on a cohort of various tumor entities (larynx (n = 19), breast (n = 18), colon (n = 4) and lung carcinoma (n = 6)) and did not refer back to entity and/or subtype specific characteristics<sup>22</sup>. Laguens *et al.* correlated their data with a pool of LN specimens from cancer-free patients while we performed a meta-analysis over all LNs due to the lack of LNs from patients without immunomodulating

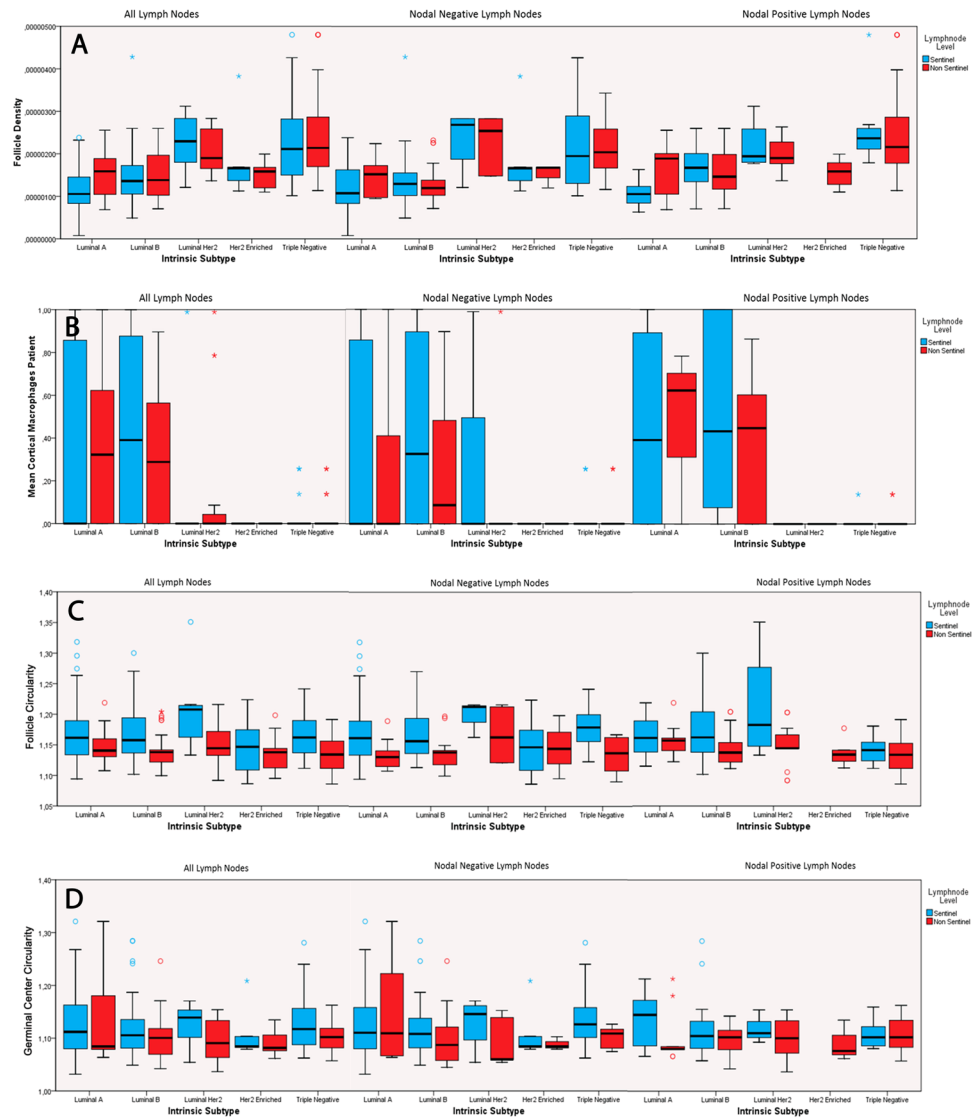


**Figure 2.** Intrinsic subtypes show differences in follicular densities (A), cortical macrophage infiltrations (B), follicular and germinal center shape (C,D); value = 1 means a perfect circle, higher values mean more irregular structures). Boxplots show median values, 66% percentiles and standard deviations, respectively. Absolute numbers of patients are highlighted in Table 4. Data underlying B was dichotomous as cortical macrophages present (=1) or absent (=0), leading to values between 0 and 1, with a possible median value = 0.

	All		Nodal Negative Lymph Nodes		Nodal Positive Lymph Nodes	
	Sentinel	Non Sentinel	Sentinel	Non Sentinel	Sentinel	Non Sentinel
Luminal A	60	26	50	15	10	11
Luminal B	59	40	41	12	18	28
Luminal Her2	8	19	4	5	4	14
Her2 enriched	8	10	7	2	1	8
Triple negative	26	50	19	16	7	34
Total	161	145	121	50	40	95

**Table 4.** Absolute numbers of patients with regard to the lymphnode level (sentinel or non-sentinel) and immunohistological subtype.

diseases (“silent LNs”) - a condition virtually absent in regional LN resection specimens. Lee *et al.* gave insights in the T-cell compartment as well as CD1a+ dendritic cell infiltrations of tumor draining LNs in breast cancer<sup>18</sup>. The latter were found to be increased in metastasis-free tumor draining axillary LNs of nodal positive cases and

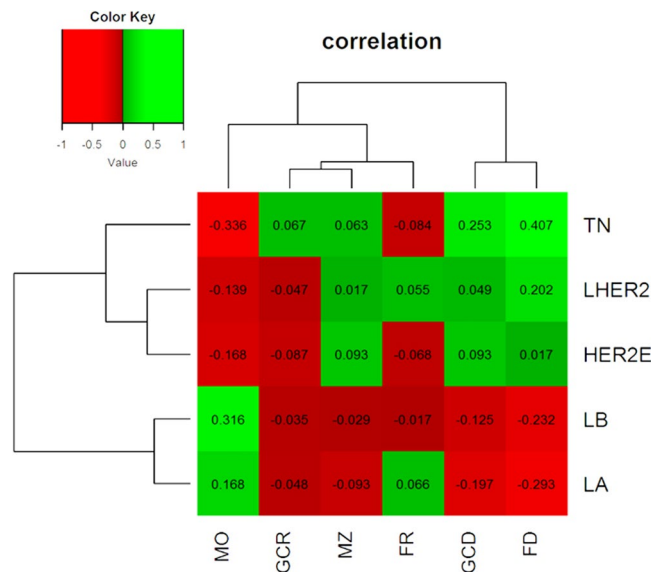


**Figure 3.** Heatmap of correlation coefficients shows subtype specific immunomorphological patterns. Parameters on the Y-axis: cortical macrophage infiltration (MO), non-circular germinal centers (GCR), mantle zone (MZ), non-circular follicles (FR), germinal center density (GCD) and follicle density (FD). Intrinsic subtypes are shown on the Y-axis: triple-negatives (TN), luminal-Her2 (LHER2), Her2-enriched (HER2E), luminal-B (LB) and luminal-A (LA).

	Follicle Density	Germinal Center Density	Non-circular Follicles	Non-circular Germinal Center	Mantle Zone Ratio	M $\phi$
Sentinel vs Level I-III (all subtypes)	<b>p = 0.001</b> cc = 0.105	p = 0.077 cc = 0.101	<b>p &lt; 0.001</b> cc = -0.409	<b>p &lt; 0.001</b> cc = -0.333	p = 0.78 cc = 0.101	<b>p &lt; 0.001</b> cc = -0.216
Sentinel vs Level I-III luminal-A	p = 0.083 cc = 0.203	p = 0.744 cc = 0.039	<b>p = 0.02</b> cc = -0.27	<b>p = 0.013</b> cc = -0.312	p = 0.449 cc = 0.089	p = 0.795 cc = 0.031
Sentinel vs Level I-III luminal-B	p = 0.451 cc = 0.08	p = 0.978 cc = -0.003	<b>p &lt; 0.001</b> cc = -0.508	<b>p = 0.008</b> cc = -0.299	p = 0.679 cc = 0.044	<b>p = 0.019</b> cc = -0.246
Sentinel vs Level I-III luminal-HER2	p = 0.569 cc = -0.115	p = 0.467 cc = 0.146	<b>p = 0.004</b> cc = -0.531	p = 0.133 cc = -0.331	p = 0.099 cc = 0.324	p = 0.813 cc = -0.048
Sentinel vs Level I-III HER2-enriched	p = 0.609 cc = -0.129	p = 0.956 cc = -0.011	p = 0.494 cc = -0.172	p = 0.102 cc = -0.424	p = 0.702 cc = 0.097	No cortical macrophages present
Sentinel vs Level I-III triple-negative	p = 0.565 cc = 0.067	p = 0.737 cc = -0.039	<b>p &lt; 0.001</b> cc = -0.508	<b>p &lt; 0.001</b> cc = -0.475	p = 0.641 cc = -0.054	p = 0.987 cc = 0.002

**Table 5.** Level stratified univariate analyses in each subtype for all patients. Spearman Rho correlation coefficient (cc) calculation was performed for all items (p value is provided over the cc value). Follicle density and germinal center density were calculated by number of follicles or germinal centers over lymph node area; calculation of non-circular follicles and germinal centers is described in the methods part; mantle zone ratio was calculated as area ratio of each germinal center over the corresponding follicle; M $\phi$ : cortical macrophage infiltrations as defined in the methods part.

even those cases without any metastasis. Our results support both studies. Furthermore, taking into account the whole group of macrophages, we were able to expand the perspective to each intrinsic subtype for the whole compartment of macrophages outside sinuses infiltrating the LN cortex, indicative for their potential of antigen presentation<sup>23,24</sup>. Higher cortical macrophage infiltrations were strongly associated with the intrinsic luminal-A and -B subtypes (Table 1., correlation subtype and macrophages  $p < 0.001$ , correlation ER/PR and macrophages  $p < 0.001$ ) and correlated with lower follicular densities in their draining LNs compared to higher follicular densities and lower cortical macrophage infiltrations in the Her2-enriched and the triple-negative subtype. This distribution of macrophages in LNs of the luminal-A and -B subtypes weakly resembles the pattern in dermatopathic lymphadenopathy, which has been described in tumor draining LNs of breast cancer as early as 1975<sup>25</sup>. We did not find significant correlations between increased cortical macrophages and nodal status (Table 1., correlation pN and macrophages  $p = 0.330$ ). Separated analysis of nodal positive and nodal negative cases showed cortical macrophages being present in both states and therefore we do not believe them to be protective – at least regarding the luminal subtypes. There are interesting functional data from mouse models claiming migratory dendritic cells from the skin mediate downregulation of cellular immune responses after protein vaccine<sup>26</sup>, which might be a mechanism behind local immune tolerance in the luminal subtypes.

Mentioning another form of LN's involvement by macrophages, sarcoid like lesions were described as pathomorphological findings in tumor draining LNs of different malignancies, including one case of breast cancer More than 60 years ago<sup>17</sup>. However, granulomas/sarcoid-like lesions were rare findings in our cohort, being present in only 4 cases (data not shown). The observation of higher cortical macrophage infiltrations inversely correlates with follicular density (highlighted by IgD staining) in our cohort, which possibly hints towards opposing mechanisms influencing the lymph nodes' population. Murine data showed IgD positive naïve B-cells (and memory B-cells) populate lymph node follicles via the CD62L/CCR7/CXCR4 mediated passage of high endothelial venules and then further through CXCR5 signaling<sup>27–29</sup>. The egress is dependent on a sphingosine 1-phosphate gradient, with high levels of sphingosine 1-phosphate in blood and lymph vessels<sup>30,31</sup>. Therefore, lowered B-cell immigration or increased egress would be dependent on the modulation of the aforementioned receptors and factors. Whether it might be beneficial to antagonize the egress of lymphocytes (e.g. with FTY720/Fingolimod)<sup>32</sup> in draining lymph nodes of hormone receptor positive breast cancers remains to be experimentally proven e.g. in animal models or by studying the draining lymph node histology under conditions of therapeutic hormone ablation. On the other hand, macrophages and their derivatives (especially dendritic cells) are – beyond their key role as antigen presenting cells – strong regulators of the amount and function of high endothelial venules<sup>33–35</sup>. However, differently polarized macrophages (M1 vs. M2) may differently modulate the vasculature also in lymph nodes so further characterization of the macrophage populations in the tumor draining lymph nodes is necessary prior to experimentally address the potential role of e.g. antiangiogenic immunomodulatory drugs<sup>36,37</sup>. Another possibility could be the direct depletion of macrophages, which has experimentally been undertaken in tumors<sup>38,39</sup>. However, this could affect also antitumoral macrophages, leading to lower survival rates<sup>40</sup>. An elegant way to recruit macrophages for an antitumoral response starts at its very beginning through activating pattern recognition receptors as e.g. TLR9<sup>40</sup>. Those therapies may also have an impact on the composition of macrophages and lymphocytes in the tumor draining lymph nodes, which yet remains to be characterized.

Setiadi *et al.* analyzed the spatial distribution of B- and T-cells in sentinel and non-sentinel LNs of 15 breast cancer (without referencing UICC classification and intrinsic subtypes) patients and identified B-cells to be more clustered than T-cells in the tumor draining LNs compared to controls<sup>19</sup>. This clustering was more prominent in axillary LNs with metastasis, followed by metastasis-free axillary LNs, followed by sentinel LNs with metastasis. In accordance with this finding, our data showed the follicular density being higher in nodal positive cases (Table 1) and in non-sentinel LNs (Table 4) in the univariate analysis. We identified lower follicular densities in LNs from the luminal-A and -B subtype. In contrast, the luminal-Her2 and triple-negative subtypes demonstrated higher follicular densities. Of note, follicular densities between sentinel and non-sentinel LNs were comparable in all groups except the luminal-A subtype with trend towards lower follicular density in the sentinel LN (Tables 3 and 5, Fig. 2A). These observations are supported by data from oral squamous cell carcinoma, with higher reactive follicle numbers being associated with better overall survival<sup>21,41</sup>. In our study, the number of disease-associated deaths was too low to identify independent effects on the patients' overall survival. Only pT- category and intrinsic subtype were significant independent prognosticators in multivariate analysis. However, the luminal-Her2 and the triple-negative subtype – both showed higher follicular densities – are more aggressive cancers<sup>42</sup>. In comparison with the aforementioned head and neck LN findings<sup>21,22</sup>, our data emphasizes that specific tumor-dependent protective immunomorphological patterns are not necessarily transferable onto other tumor entities.

Comparing tumor draining LNs and the primary tumor site, the triple-negative subtype resembles the luminal-Her2 subtype in follicular density and shape, whereas tumor infiltrating lymphocytes are a dominant feature of only the triple-negative subtype (Table 3). To our knowledge, there are currently no available comparative results of immunomodulatory therapies in triple-negative and luminal-Her2 breast cancer to postulate whether there is a similar (mirroring similar LN findings) or different therapeutic response (mirroring different TIL infiltration). This information may perhaps be extracted from ongoing and planned future studies summarized by Spellman and Tang<sup>43</sup>.

Little is known about the shape of follicles and germinal centers in tumor draining LNs. Berlinger *et al.* described reactive follicles with germinal centers tending to “fuse” in tumor draining LNs of head and neck squamous cell carcinoma<sup>41</sup>. Regarding the microphotographies of this paper, these “fused” germinal centers are the same we classified as non-circular in this actual and a previous study<sup>44</sup>. Non-circular germinal centers can be found in infectious lymphadenopathies as toxoplasmosis, EBV and HIV<sup>45–48</sup>. Further associations exist with Common Variable Immunodeficiency (CVID) – especially those of the Freiburg class Ia group with stronger immune dysregulation<sup>44</sup>, and angioimmunoblastic T-cell lymphoma<sup>49–51</sup>. The functional background shaping this germinal center morphology remains elusive but there is experimental data indicating a role of higher interferon gamma levels in CVID patients<sup>52</sup>.

Follicular helper T cells (T<sub>fh</sub>) play an essential role in the germinal center formation, maintenance and output, e.g. through mediating the class switch recombination of germinal center B-cells<sup>53</sup>. T<sub>fh</sub> express PD1 and are pronounced in the light zone of the germinal centers<sup>54,55</sup>. Data in mice indicate PD1 signaling being important for the germinal center output of long lived, class switched plasma cells as well as immunoglobulin levels and affinities<sup>56–59</sup>. However, results are heterogenous as different costimulatory molecules and points in time were observed in the different groups. The impact of PD1 inhibitor therapy on germinal center morphology has not been described to date. Cytotoxic T-lymphocyte-associated Protein 4 (CTLA4) as a further therapeutic target of immune checkpoint inhibition plays an important role for T<sub>fh</sub> function and the germinal center's shape<sup>60</sup>. CTLA4 antagonization or deficiency is associated with large, ill-defined germinal centers and lowered serum immunoglobulin levels<sup>60,61</sup>.

Evaluating the germinal center size and shape may therefore be a potential predictive marker to better define patients who would benefit from therapies targeting immune checkpoints, as intra- and peritumoral genetic and/or immunohistochemical markers alone are not sufficient to predict therapeutic outcome yet<sup>62–64</sup>. Based on our findings and the published data discussed, we hypothesize an increased benefit from immune checkpoint inhibition in patients with high densities of germinal centers with a round shape in their tumor draining lymph nodes.



To conclude, we show that breast cancer subtype-specific immunomorphological changes reflecting different underlying immunomodulations take place in the tumor draining LNs. These immunomorphological changes may help to study the patients' immune resources beyond the primary site and may help to guide patient selection to immunomodulatory drug treatment. Further studies in tumor draining LNs are necessary to characterize the functional background of those different immunomorphologies for their therapeutic targeting in the future.

## Material and Methods

**Patients and cohort.** After ethics approval by local authorities (Ethics Committee University Medical Center Freiburg; voted application number 10011/16) according to the Helsinki declaration, matching tumor and regional LN samples of 206 patients (operated between 2003 to 2013) were retrieved from the local biobank. Surgery for primary breast cancer and corresponding LNs was performed at the Department of Obstetrics and Gynecology at the University Medical Center Freiburg. Inclusion criteria were existing sentinel LN, absence of neoadjuvant therapy and absence of anti-hormonal treatment prior to resection. All surgically removed LN samples were assigned according to their LN level (sentinel, level I, level II, and level III). Of note, all tumors were histologically and immunohistologically classified according to their WHO subtype<sup>65</sup>, tumor grading (Elston and Ellis)<sup>66</sup>, the expression of estrogen and progesterone receptor proteins<sup>67</sup>, MIB-1 based proliferation index, and human epidermal growth factor receptor 2 (Her2neu)<sup>68</sup> expression. In case of Her2neu score 2+, chromogenic *in situ* hybridization was performed. Subsequently, all tumors were classified with respect to their molecular subtype (luminal-A, luminal-B, luminal-Her2, Her2-enriched, and triple-negative) according to the 2011 St. Gallen guidelines<sup>69</sup>. Patients' characteristics are listed in Table 1.

**H&E/IgD Staining.** For the observation of B-cell follicles, mantle zones, germinal centers, and LN morphology, H&E/IgD "double" staining was performed. Slides of 2  $\mu\text{m}$  were dried at 58 °C overnight and deparaffinized in xylene and decreasing ethanol concentrations. Heat-mediated epitope retrieval was performed for 20 minutes at pH 6.1 and 95 °C. Slides were stained with hematoxylin before further proceeding with IgD staining. IgD immunohistochemistry was performed on an automated staining system using a horseradish peroxidase catalyzed brown chromogen reaction according to the manufacturer's guidelines (antibody: polyclonal rabbit anti-human IgD, IS51730-2, ready to use, Dako, Hamburg, Germany; staining: Autostainer Plus, Dako). The slide was then stained with Eosin Y (Leica Biosystems, Nussloch, Germany) and covered with a coverslip.

**Estrogen, Progesterone, Her2 and Ki67 Staining.** The intrinsic subtype was immunohistologically identified via ready-to-use antibodies for the estrogen-receptor protein (monoclonal rabbit anti-human estrogen receptor  $\alpha$ , clone EP1, code IR084, Dako) progesterone-receptor protein (monoclonal mouse anti-human progesterone receptor, clone PgR 636, code IR068, Dako), Her2 (polyclonal rabbit anti-human c-erbB-2 oncoprotein, code A0485, Dako) and Ki-67 (monoclonal mouse anti-human Ki-67 antigen, clone MIB-1, code IR626, Dako). For the horse-radish based peroxidase detection, EnVision Flex Peroxidase-Blocking Reagent (DAKO, SM801), EnVision Flex+ Rabbit (LINKER) (DAKO, K8019) or EnVision Flex+ Mouse (LINKER) (DAKO, K8021) and EnVision Flex/HRP (DAKO, SM802) were used. Counterstaining was performed with hematoxylin before adding the coverslip.

As an internal positive control, patient-derived, non-neoplastic mammary glands were used for ER, PR and Ki-67 (nuclear staining). For Her2, tissue specimens from Her2 positive breast cancer patients (score 3 according to Wolff *et al.*<sup>68</sup>) were included for every Her2 staining session as external positive control.

**Slide Scanning and Evaluation of LNs.** Morphometrical analysis was performed on digitized slides (detailed workflow is presented in Fig. 4). All slides were annotated with a unique identifier, scanned with a 20  $\times$  objective (Mirax Scan Panoramic Scanner, 3DHistec, Hungary) and analyzed using the manufacturer's proprietary software (Panoramic Viewer, version 1.15.4, 3DHistec). B-cell follicles and matching germinal centers, LNs and (if present) metastases were individually annotated and parsed for each LN separately using the software's annotation function. Circumferences and areas of the named structures were exported as.csv file (Panoramic Viewer, version 1.15.4, 3DHistec) for further quantitative analysis: number and area of LNs and metastases as well as number, area, circumference and circularity of follicles and matching germinal centers. Roundness of germinal centers and follicles was calculated as previously described<sup>44</sup>. Briefly, radii of follicle and germinal center were calculated from circumference and area and put into ratio. A ratio of one represents a perfect circle – in our case a round follicle and/or germinal center – a ratio >1 represents a non-circular structure – in our case a non-circular follicle and/or germinal center. Mantle zones were calculated as ratio of germinal center area divided through follicle area. LN cortical macrophage infiltration was measured semi-quantitatively in each LN as infiltration of follicular and inter-follicular areas (sinuses were excluded): three spots of macrophage-rich cortical infiltration (diameter of 1 HPF, digital 40x magnification on 17" screen) or one spot in a 20x field diameter. Cortical macrophages were graded per LN as either present (=1) or absent (=0).

Follicular and germinal center density was calculated as numbers of follicles and germinal centers divided by the area of the corresponding LN.

Mantle zone was calculated by dividing germinal center area by follicle area.

Regarding primary tumors, lymphocytic infiltrations in tumors were measured semiquantitatively on H&E sections with conventional microscopy. Tumors were considered "lymphocyte rich" if coherent lymphocytic infiltrates were visible in 20x field of view (microscope: Leica DM 2500, Wetzlar, Germany).

All annotations were continuously reviewed and discussed by two experienced pathologists until consensus was reached. Until consensus, the pathologists were blinded for all clinicopathological parameters.

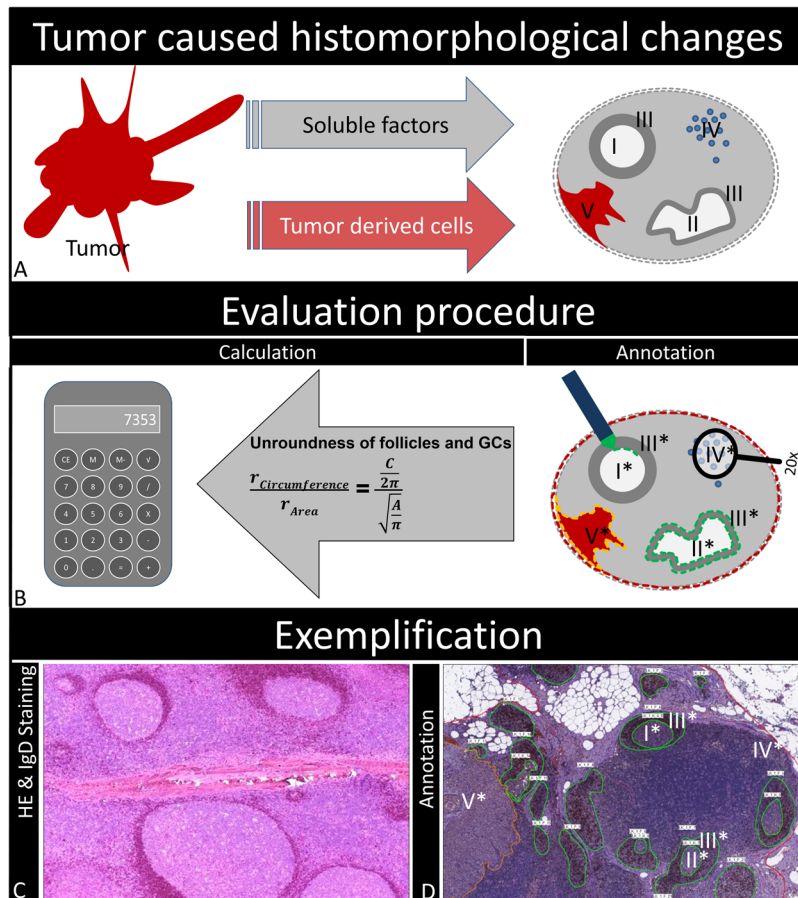


**Figure 4.** Workflow. (A) Tumor and matching lymph nodes were included and analyzed based on anatomic immunological structures: Germinal centers (I round, II non-circular), follicles and germinal center mantle zones (III), cortical macrophage infiltrations (IV) and lymph node metastasis (V). (B) Structures were annotated for further calculations as area densities and roundness. (C) H&E/IgD stainings were performed on all lymph nodes to highlight the structures. (D) Example of fully annotated H&E stained lymph node section.

**Statistical Analysis.** For descriptive statistics and statistical testing, SPSS version 21 (IBM SPSS Inc, Chicago, IL, U.S.A.) was used. Scale variables were expressed as median and range, categorical parameters by cross tabulation and percentages. For statistical testing, two-sided Chi-squared, Mann-Whitney, Spearman rank correlation and logistic regression models were performed. A significance level of 5% was chosen. Heatmap and Clustering were performed with the R package gplots 3.31.

## References

- Cochran, A. J. *et al.* Tumour-induced immune modulation of sentinel lymph nodes. *Nat. Rev. Immunol.* **6**, 659–670 (2006).
- Mueller, S. N. & Germain, R. N. Stromal cell contributions to the homeostasis and functionality of the immune system. *Nat. Rev. Immunol.* **9**, 618–29 (2009).
- Yang, C.-Y. *et al.* Trapping of naive lymphocytes triggers rapid growth and remodeling of the fibroblast network in reactive murine lymph nodes. *Proc. Natl. Acad. Sci. USA* **111**, E109–18 (2014).
- Weiss, L. M. & O'Malley, D. Benign lymphadenopathies. *Mod. Pathol.* **26**, S88–S96 (2013).
- Toccanier-Pelte, M. F., Skalli, O., Kapanci, Y. & Gabbiani, G. Characterization of stromal cells with myoid features in lymph nodes and spleen in normal and pathologic conditions. *Am. J. Pathol.* **129**, 109–18 (1987).
- Muñoz-Fernández, R. *et al.* Follicular dendritic cells are related to bone marrow stromal cell progenitors and to myofibroblasts. *J. Immunol.* **177**, 280–9 (2006).
- Chung, M. K. *et al.* Lymphatic Vessels and High Endothelial Venules are Increased in the Sentinel Lymph Nodes of Patients with Oral Squamous Cell Carcinoma Before the Arrival of Tumor Cells. *Ann. Surg. Oncol.* **19**, 1595–1601 (2012).
- Qian, C.-N. *et al.* Preparing the “soil”: the primary tumor induces vasculature reorganization in the sentinel lymph node before the arrival of metastatic cancer cells. *Cancer Res.* **66**, 10365–76 (2006).
- Hirakawa, S. *et al.* VEGF-A induces tumor and sentinel lymph node lymphangiogenesis and promotes lymphatic metastasis. *J. Exp. Med.* **201**, 1089–1099 (2005).
- Hirakawa, S. *et al.* VEGF-C-induced lymphangiogenesis in sentinel lymph nodes promotes tumor metastasis to distant sites. *Blood* **109**, 1010–1017 (2006).
- Müller, A. *et al.* Involvement of chemokine receptors in breast cancer metastasis. *Nature* **410**, 50–56 (2001).
- Coghlin, C. & Murray, G. I. Current and emerging concepts in tumour metastasis. *J. Pathol.* **222**, 1–15 (2010).
- Paget, S. The distribution of secondary growths in cancer of the breast. *Lancet* **133**, 571–573 (1889).
- Pereira, E. R., Jones, D., Jung, K. & Padera, T. P. The lymph node microenvironment and its role in the progression of metastatic cancer. *Semin. Cell Dev. Biol.* **38**, 98–105 (2015).

15. Chodon, T., Koya, R. C. & Odunsi, K. Active Immunotherapy of Cancer. *Immunol. Invest.* **44**, 817–836 (2015).
16. Ma, W., Gilligan, B. M., Yuan, J. & Li, T. Current status and perspectives in translational biomarker research for PD-1/PD-L1 immune checkpoint blockade therapy. *J. Hematol. Oncol.* **9**, 47 (2016).
17. Nadel, E. M. & Ackerman, L. V. Lesions resembling Boeck's sarcoid in lymph nodes draining an area containing a malignant neoplasm. *Am. J. Clin. Pathol.* **20**, 952–7 (1950).
18. Kohrt, H. E. *et al.* Profile of immune cells in axillary lymph nodes predicts disease-free survival in breast cancer. *PLoS Med.* **2**, e284 (2005).
19. Setiadi, A. F. *et al.* Quantitative, architectural analysis of immune cell subsets in tumor-draining lymph nodes from breast cancer patients and healthy lymph nodes. *PLoS One* **5**, e12420 (2010).
20. Riazi Rad, F., Ajdary, S., Omranipour, R., Alimohammadian, M. H. & M Hassan, Z. Comparative Analysis of CD4+ and CD8+ T Cells in Tumor Tissues, Lymph Nodes and the Peripheral Blood from Patients with Breast Cancer. *Iran. Biomed. J.* **19**, 35–44 (2015).
21. Vered, M. *et al.* Key architectural changes in tumor-negative lymph nodes from metastatic-free oral cancer patients are valuable prognostic factors. *Clin. Exp. Metastasis* **31**, 327–38 (2014).
22. Laguens, G., Coronato, S., Laguens, R., Portiansky, E. & Di Girolamo, V. Human regional lymph nodes draining cancer exhibit a profound dendritic cell depletion as comparing to those from patients without malignancies. *Immunol. Lett.* **84**, 159–162 (2002).
23. Cyster, J. G. B cell follicles and antigen encounters of the third kind. *Nat. Immunol.* **11**, 989–996 (2010).
24. Gasteiger, G., Ataide, M. & Kastenmüller, W. Lymph node - an organ for T-cell activation and pathogen defense. *Immunol. Rev.* **271**, 200–220 (2016).
25. Ree, H. & Fanger, H. Paracortical alteration in lymphadenopathic and tumor-draining lymph nodes: histologic study. *Hum. Pathol.* **6**, 363–72 (1975).
26. Anandasabapathy, N. *et al.* Classical Flt3L-dependent dendritic cells control immunity to protein vaccine. *J. Exp. Med.* **211**, 1875–91 (2014).
27. Park, C. *et al.* Lymph node B lymphocyte trafficking is constrained by anatomy and highly dependent upon chemoattractant desensitization. *Blood* **119**, 978–89 (2012).
28. Okada, T. *et al.* Chemokine requirements for B cell entry to lymph nodes and Peyer's patches. *J. Exp. Med.* **196**, 65–75 (2002).
29. Förster, R. *et al.* CCR7 coordinates the primary immune response by establishing functional microenvironments in secondary lymphoid organs. *Cell* **99**, 23–33 (1999).
30. Cyster, J. G. Chemokines, Sphingosine-1-Phosphate, And Cell Migration In Secondary Lymphoid Organs. *Annu. Rev. Immunol.* **23**, 127–159 (2005).
31. Thangada, S. *et al.* Cell-surface residence of sphingosine 1-phosphate receptor 1 on lymphocytes determines lymphocyte egress kinetics. *J. Exp. Med.* **207**, 1475–83 (2010).
32. Chiba, K. *et al.* FTY720, a novel immunosuppressant, induces sequestration of circulating mature lymphocytes by acceleration of lymphocyte homing in rats. I. FTY720 selectively decreases the number of circulating mature lymphocytes by acceleration of lymphocyte homing. *J. Immunol.* **160**, 5037–44 (1998).
33. Samlowski, W. E., Chung, H. T., Burnham, D. K. & Daynes, R. A. Regional immunology The role of macrophages in the regulation of high endothelial venule expression within the peripheral lymph nodes of mice exposed to ultraviolet radiation. *Reg. Immunol.* **1**, 41–55 (1988).
34. Hendriks, H. R. & Eestermans, I. L. Disappearance and reappearance of high endothelial venules and immigrating lymphocytes in lymph nodes deprived of afferent lymphatic vessels: a possible regulatory role of macrophages in lymphocyte migration. *Eur. J. Immunol.* **13**, 663–669 (1983).
35. Ager, A. High Endothelial Venules and Other Blood Vessels: Critical Regulators of Lymphoid Organ Development and Function. *Front. Immunol.* **8**, 45 (2017).
36. Tsutsui, S. *et al.* Macrophage infiltration and its prognostic implications in breast cancer: the relationship with VEGF expression and microvessel density. *Oncol. Rep.* **14**, 425–31 (2005).
37. Goswami, K. K. *et al.* Tumor promoting role of anti-tumor macrophages in tumor microenvironment. *Cell. Immunol.* **316**, 1–10 (2017).
38. Zeisberger, S. M. *et al.* Clodronate-liposome-mediated depletion of tumour-associated macrophages: a new and highly effective antiangiogenic therapy approach. *Br. J. Cancer* **95**, 272–81 (2006).
39. Priceman, S. J. *et al.* Targeting distinct tumor-infiltrating myeloid cells by inhibiting CSF-1 receptor: combating tumor evasion of antiangiogenic therapy. *Blood* **115**, 1461–71 (2010).
40. Schaedler, E. *et al.* Sequential administration of a MVA-based MUC1 cancer vaccine and the TLR9 ligand Litenimod (Li28) improves local immune defense against tumors. *Vaccine* **35**, 577–585 (2017).
41. Berlinger, N. T. *et al.* Immunologic assessment of regional lymph node histology in relation to survival in head and neck carcinoma. *Cancer* **37**, 697–705 (1976).
42. Metzger-Filho, O. *et al.* Patterns of Recurrence and Outcome According to Breast Cancer Subtypes in Lymph Node-Negative Disease: Results From International Breast Cancer Study Group Trials VIII and IX. *J. Clin. Oncol.* **31**, 3083–3090 (2013).
43. Spellman, A. & Tang, S.-C. Immunotherapy for breast cancer: past, present, and future. *Cancer Metastasis Rev.* **35**, 525–546 (2016).
44. Unger, S. *et al.* Ill-Defined Germinal Centers and Severely Reduced Plasma Cells are Histological Hallmarks of Lymphadenopathy in Patients with Common Variable Immunodeficiency. *J. Clin. Immunol.* <https://doi.org/10.1007/s10875-014-0052-1> (2014).
45. Kojima, M. *et al.* Infectious mononucleosis lymphadenitis showing histologic findings indistinguishable from toxoplasma lymphadenitis. A report of three cases. *Pathol. Res. Pract.* **206**, 361–4 (2010).
46. Kojima, M., Kitamoto, Y., Shimizu, K., Matsuda, H. & Masawa, N. Tonsillar lesions of infectious mononucleosis resembling MALT type lymphoma. A report of two cases. *Pathol. Oncol. Res.* **14**, 489–92 (2008).
47. Turner, R. R., Levine, A. M., Gill, P. S., Parker, J. W. & Meyer, P. R. Progressive histopathologic abnormalities in the persistent generalized lymphadenopathy syndrome. *Am. J. Surg. Pathol.* **11**, 625–32 (1987).
48. Gujral, S. *et al.* Study of the morphological patterns and association of Epstein-Barr virus and human herpes virus 8 in acquired immunodeficiency deficiency syndrome-related reactive lymphadenopathy. *Indian J. Pathol. Microbiol.* **53**, 723–8.
49. Kojima, M. *et al.* Angioimmunoblastic T-cell lymphoma with hyperplastic germinal centers: a clinicopathological and immunohistochemical study of 10 cases. *APMIS* **109**, 699–706 (2001).
50. Ree, H. J. *et al.* Angioimmunoblastic lymphoma (AILD-type T-cell lymphoma) with hyperplastic germinal centers. *Am. J. Surg. Pathol.* **22**, 643–55 (1998).
51. Ree, H. J. *et al.* Bcl-6 expression in reactive follicular hyperplasia, follicular lymphoma, and angioimmunoblastic T-cell lymphoma with hyperplastic germinal centers: heterogeneity of intrafollicular T-cells and their altered distribution in the pathogenesis of angioimmunol. *Hum. Pathol.* **30**, 403–11 (1999).
52. Unger, S. *et al.* TH1 phenotype of T follicular helper cells indicates an IFN $\gamma$ -associated immune dysregulation in CD21low CVID patients. *J. Allergy Clin. Immunol.* <https://doi.org/10.1016/j.jaci.2017.04.041> (2017).
53. Qi, H. T follicular helper cells in space-time. *Nat. Rev. Immunol.* **16**, 612–625 (2016).
54. Haynes, N. M. *et al.* Role of CXCR5 and CCR7 in follicular Th cell positioning and appearance of a programmed cell death gene-high germinal center-associated subpopulation. *J. Immunol.* **179**, 5099–108 (2007).
55. Iwai, Y. *et al.* Microanatomical localization of PD-1 in human tonsils. *Immunol. Lett.* **83**, 215–20 (2002).

56. Good-Jacobson, K. L. *et al.* PD-1 regulates germinal center B cell survival and the formation and affinity of long-lived plasma cells. *Nat. Immunol.* **11**, 535–542 (2010).
57. Hamel, K. M. *et al.* B7-H1 expression on non-B and non-T cells promotes distinct effects on T- and B-cell responses in autoimmune arthritis. *Eur. J. Immunol.* **40**, 3117–3127 (2010).
58. Kawamoto, S. *et al.* The inhibitory receptor PD-1 regulates IgA selection and bacterial composition in the gut. *Science* **336**, 485–9 (2012).
59. Hams, E. *et al.* Blockade of B7-H1 (Programmed Death Ligand 1) Enhances Humoral Immunity by Positively Regulating the Generation of T Follicular Helper Cells. *J. Immunol.* **186**, 5648–5655 (2011).
60. Wang, C. J. *et al.* CTLA-4 controls follicular helper T-cell differentiation by regulating the strength of CD28 engagement. *Proc. Natl. Acad. Sci. USA* **112**, 524–9 (2015).
61. Schubert, D. *et al.* Autosomal dominant immune dysregulation syndrome in humans with CTLA4 mutations. *Nat. Med.* **20**, 1410–6 (2014).
62. Hamid, O. *et al.* Safety and Tumor Responses with Lambrolizumab (Anti-PD-1) in Melanoma. *N. Engl. J. Med.* **369**, 134–144 (2013).
63. Powles, T. *et al.* Updated European Association of Urology Guidelines Recommendations for the Treatment of First-line Metastatic Clear Cell Renal Cancer. *Eur. Urol.* <https://doi.org/10.1016/j.eururo.2017.11.016> (2017).
64. Rossfeld, K. *et al.* Metastatic melanoma patients' sensitivity to ipilimumab cannot be predicted by tumor characteristics. *Int. J. Surg. Oncol.* **2**, e43 (2017).
65. IARC Publications - Pathology and Genetics of Tumours of the Breast and Female Genital Organs. at <http://www.iarc.fr/en/publications/pdfs-online/pat-gen/bb4/>.
66. Elston, C. W. & Ellis, I. O. Pathological prognostic factors in breast cancer. I. The value of histological grade in breast cancer: experience from a large study with long-term follow-up. *Histopathology* **19**, 403–10 (1991).
67. Hammond, M. E. H., Hayes, D. F., Wolff, A. C., Mangu, P. B. & Temin, S. American society of clinical oncology/college of american pathologists guideline recommendations for immunohistochemical testing of estrogen and progesterone receptors in breast cancer. *J. Oncol. Pract.* **6**, 195–7 (2010).
68. Wolff, A. C. *et al.* American Society of Clinical Oncology/College of American Pathologists guideline recommendations for human epidermal growth factor receptor 2 testing in breast cancer. *Arch. Pathol. Lab. Med.* **131**, 18–43 (2007).
69. Goldhirsch, A. *et al.* Strategies for subtypes—dealing with the diversity of breast cancer: highlights of the St. Gallen International Expert Consensus on the Primary Therapy of Early Breast Cancer 2011. *Ann. Oncol.* **22**, 1736–47 (2011).

## Acknowledgements

50% of the position of Maximilian Seidl was funded by the Comprehensive Cancer Center Freiburg for the duration of 12 months. Consumables were partly funded by the German Society for Pathology.

## Author Contributions

Maximilian Seidl: study design, data collection, statistics, data interpretation, literature research, writing of manuscript, critical review of the manuscript. Moritz Bader: data collection, data interpretation. Astrid Vaihinger: data collection, data interpretation. Ulrich F. Wellner: statistics, data interpretation. Romyana Todorova: data collection, data interpretation. Bettina Herde: sample preparation, immunohistochemistry. Klaudia Schrenk: sample preparation, immunohistochemistry. Jochen Maurer: technical support, literature research, writing of the manuscript. Oliver Schilling: literature research, writing of the manuscript. Thalia Erbes: clinical data, technical support. Paul Fisch: writing of the manuscript, critical review of the manuscript. Jens Pfeiffer: writing of the manuscript, technical support. Linda Hoffmann: data collection, statistics. Kai Franke: data collection, statistics. Martin Werner: data interpretation, writing of the manuscript, critical review of the manuscript. Peter Bronsert: study design, data collection, statistics, data interpretation, literature research, writing of manuscript, critical review of the manuscript.

## Additional Information

**Competing Interests:** The authors declare no competing interests.

**Publisher's note:** Springer Nature remains neutral with regard to jurisdictional claims in published maps and institutional affiliations.



**Open Access** This article is licensed under a Creative Commons Attribution 4.0 International License, which permits use, sharing, adaptation, distribution and reproduction in any medium or format, as long as you give appropriate credit to the original author(s) and the source, provide a link to the Creative Commons license, and indicate if changes were made. The images or other third party material in this article are included in the article's Creative Commons license, unless indicated otherwise in a credit line to the material. If material is not included in the article's Creative Commons license and your intended use is not permitted by statutory regulation or exceeds the permitted use, you will need to obtain permission directly from the copyright holder. To view a copy of this license, visit <http://creativecommons.org/licenses/by/4.0/>.

© The Author(s) 2018